Fraction of Free-Base Nicotine in Simulated Vaping Aerosol Particles Determined by X-Ray Spectroscopies

Chaya Weeraratna[1], Xiaochen Tang[2], Oleg Kostko[1,3], Vi H. Rapp[2], Lara A. Gundel[2],

Hugo Destaillats[2,*], Musahid Ahmed[1,*]

1. *Chemical Science Division, Lawrence Berkeley National Laboratory, Berkeley, California 94720, USA*

2. *Energy Technologies Area, Lawrence Berkeley National Laboratory, Berkeley, California 94720, USA*

3. *Advanced Light Source, Lawrence Berkeley National Laboratory, Berkeley, California 94720, USA*

* Corresponding authors E-mails: MAhmed@lbl.gov; HDestaillats@lbl.gov

Abstract

A new generation of electronic cigarettes is exacerbating the youth vaping epidemic by incorporating additives that increase the acidity of generated aerosols, which facilitate uptake of high nicotine levels. We need to better understand the chemical speciation of vaping aerosols to assess the impact of acidification. Here we used X-ray photoelectron spectroscopy (XPS) and near-edge X-ray absorption fine structure (NEXAFS) spectroscopy to probe the acid-base equilibria of nicotine in hydrated vaping aerosols. We show that, unlike the behavior observed in bulk water, nicotine in the core of aqueous particles was partially protonated when the pH of the nebulized solution was 10.4, with a fraction of free-base nicotine (α_{FB}) of 0.34. Nicotine was further protonated by acidification with equimolar addition of benzoic acid (α_{FB} = 0.17 at pH 6.2). By contrast, the degree of nicotine protonation at the particle surface was significantly lower, with 0.72 < α_{FB} < 0.80 in the same pH range. The presence of propylene glycol and glycerol completely eliminated protonation of nicotine at the surface (α_{FB} = 1), while not affecting significantly its acid-base equilibrium in the particle core. These results provide a better understanding of the role of acidifying additives in vaping aerosols, supporting public health policy interventions.

TOC graphic
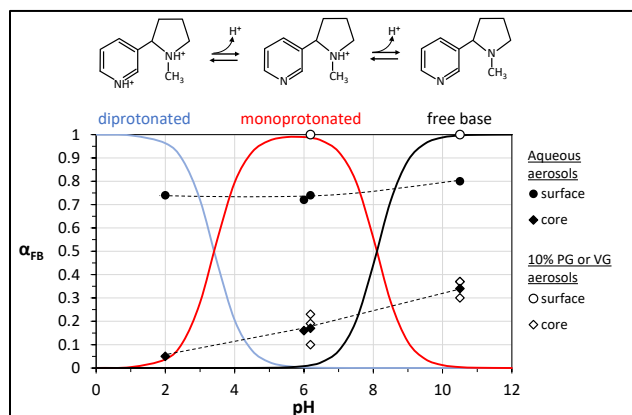
The composition of aerosols emitted by electronic cigarettes (e-cigarettes) and other emerging tobacco products has been described using traditional methods that rely on collecting samples onto sorbent tubes or filters, followed by off-line chromatographic and mass spectrometric analysis.[1-4] The two main compounds used as solvent in refill liquids (e-liquids) are propylene glycol (PG) and vegetable glycerol (VG, or glycerol) mixed in different proportions, and often combined with smaller amounts of water and ethanol. In e-liquids sold in Europe, nicotine concentration is regulated not to exceed 20 mg mL^{-1} (0.12 M), while nicotine levels in North American products were found to be as high as 69 mg mL^{-1} (0.43 M).[5-7] Multiple additives are commonly used as flavorings, from which ethyl maltol, ethyl vanillin, vanillin, cinnamaldehyde and menthol are among the most popular. Typically, these additives are present at lower concentrations than nicotine (e.g., 0.02 to 10 mg mL^{-1}).[8, 9] However, other additives are used in larger amounts to increase the acidity of aerosols. In particular, carboxylic acids (benzoic, lactic, levulinic acid) are used in some of the best-selling products at levels comparable with nicotine (molar ratio ≈ 1).[10-12] By protonating nicotine, carboxylic acids make the aerosol less harsh upon inhalation, thus enabling formulations containing up to 6 times higher nicotine levels than in comparable acid-free e-liquids. Such higher nicotine intake promotes and facilitates initiation and addiction.[13-16] Menthol is also used at similarly high concentrations to reinforce smoking behavior due to its analgesic, antitussive, soothing and expectorating properties.[17]
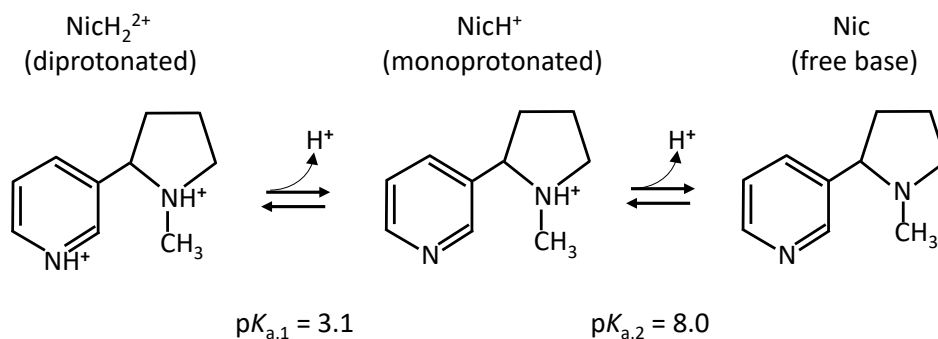
The speciation of nicotine in inhaled particles has significant implications on the delivery profile of e-cigarettes.[18] Four different mechanisms by which nicotine can deposit in the respiratory tract have been described: (1) direct deposition from the gas phase, (2) evaporation from airborne particles followed by gas phase deposition, (3) evaporation from deposited particles followed by gas phase deposition, and (4) particle deposition with subsequent diffusion of nicotine to lining fluids.[19, 20] The first three involve volatilization of free-base nicotine from the aerosol, and are influenced by its volatility. The fraction of the neutral free-base form α_{FB} in tobacco smoke is defined as [21]

$$\alpha_{FB} = \frac{[\text{Nic}]_{FB}}{[\text{Nic}]_{FB} + [\text{Nic}]_P} \qquad (1)$$

Where $[\text{Nic}]_{FB}$ and $[\text{Nic}]_P$ are the concentrations of free-base and protonated nicotine in the aerosol particles, respectively, as described in Scheme 1.

In Equation 1, $[\text{Nic}]_P$ represents the sum of monoprotonated (NicH$^+$) and diprotonated (NicH$_2^{2+}$) nicotine. However, the formation of diprotonated nicotine, with a second proton on the pyridinic nitrogen, requires very acidic conditions unlikely to be found in most vaping aerosols. A few studies measured pH and α_{FB} in e-liquids and in aerosol samples generated by heating those liquids, using indirect methods based on liquid-liquid extraction of free-base nicotine,[22-24] and direct measurements using ^{1}H-NMR.[13] In all cases, a broad range of α_{FB} values was observed among different e-liquids, even for products with similar nicotine levels. When α_{FB} was compared between values obtained on specific e-liquids and the

2

corresponding aerosol generated with them, some studies show similar α_{FB} values, but others reported significant differences.

$\begin{array}{ccc} \text{NicH}_2{}^{2+} & \text{NicH}^+ & \text{Nic} \\ \text{(diprotonated)} & \text{(monoprotonated)} & \text{(free base)} \end{array}$

$pK_{a,1} = 3.1 \qquad pK_{a,2} = 8.0$

Scheme 1: Acid-base equilibria of nicotine in aqueous solution.

Here, we explored the degree of protonation of nicotine in the surface and core of freshly-generated aerosol particles, immediately after inception. This is the most relevant time scale to describe user's uptake and secondhand exposures. Experiments evaluated acid-base equilibria in aqueous aerosols, the effects due to the presence of PG and VG, and due to interactions between nicotine and benzoic acid (BA). In experiments with PG, VG or their mixture, we tested aerosols that are highly hydrated, containing 32 – 36 wt% of those compounds (corresponding in all cases to 10% in moles), as vaping aerosols from liquids using PG and VG as solvents undergo rapid hygroscopic growth in the mouth and upper respiratory system.[25] Near-edge X-ray absorption fine structure (NEXAFS) spectroscopy was used to characterize chemical species present in the core of aerosol particles. Species at the particle surface exhibit a distinct chemical behavior, which was investigated with X-ray photoelectron spectroscopy (XPS).[26]

Aerosol generation and characterization. Simulated vaping aerosols were generated under comparable conditions as those produced with electronic cigarettes, considering the aerosol particle size distribution and aerosol concentration. The size-resolved particle number (PN), particle mass (PM) and particle surface area (PS) concentrations of generated aerosols determined as a function of particle size are presented in Figure 1. In the first column, aerosols generated by nebulizing a 0.5 M nicotine aqueous solution (pH 10.4, ionic strength 2.5 10^{-4} M) are compared with those derived from an equimolar 0.5 M aqueous mixture of nicotine and BA (pH 6.2, ionic strength 0.5 M), and 0.5 M nicotine solutions acidified by addition of HCl to pH 6 (ionic strength 0.5 M) and pH 2 (ionic strength 1.5 M). In subsequent columns,

3

we evaluated the aerosols formed from 0.5 M nicotine aqueous solutions that were modified with 10% (molar ratio) PG, 10% VG, and 10% of a PG/VG (30/70) mixture. Each of those plots include three curves, corresponding to aerosol produced by the solvent, and by 0.5 M nicotine in the absence and presence of 0.5 M BA. In all cases, aerosol concentrations were measured with instruments spanning a wide particle size range of 8 nm – 2.5 µm.

In most tested conditions, the observed particle size distribution was multimodal, and the relative prevalence of ultrafine vs. fine particles changed with the composition of the mixture. Our results are consistent with those reported for the atomization of aqueous glycerol mixtures containing different solute concentrations,[27] and with the generation of vaping aerosols using mixtures of PG, VG and nicotine in different proportions.[28] It should be noted that the PN, PM and PS concentration profiles of aerosols generated with 0.5 nicotine at pH 2 were significantly different from other conditions, with overall higher aerosol concentrations and a marked bimodal shape. This could be due to a higher concentration of ionic species; however, these acidic conditions are more extreme than those reported in vaping e-liquids and aerosols.

The 50 nm – 1 µm range corresponds to a sub-set of particles that was analyzed by X-ray techniques, represented with a blue box in each plot. The average concentration and the fraction of the total detected aerosol are summarized in Table S1 (Supporting Information). All mixtures produced a large number of ultrafine particles smaller than 50 nm, however these could not be captured by the aerodynamic lens system used for X-ray spectroscopy. The PN concentration for particles which were interrogated within the 50 nm – 1 µm range was between 2 E+06 and 6 E+07 # cm^{-3}. In most cases, these corresponded to between one and two thirds of the total particles emitted by the atomizer. The PM concentration of aerosol detected by X-ray methods was between 10 and 300 mg m^{-3}, corresponding to between 60 to 80% of the total mass of aerosol emitted, while the PS concentration was between 0.2 and 5 mm^2 cm^{-3}, corresponding to >75% of the total aerosol surface delivered by the atomizer. This is important as the X-ray techniques used in this work, particularly XPS, are extremely surface sensitive allowing us to capture the relevant chemistry of vaping aerosols. Despite the above-mentioned variability in the multimodal particle size distribution observed in different tests, we do not anticipate this effect to introduce major biases on the X-ray spectroscopic analysis, as most of the generated particle number, mass and surface concentrations were included in the tests.
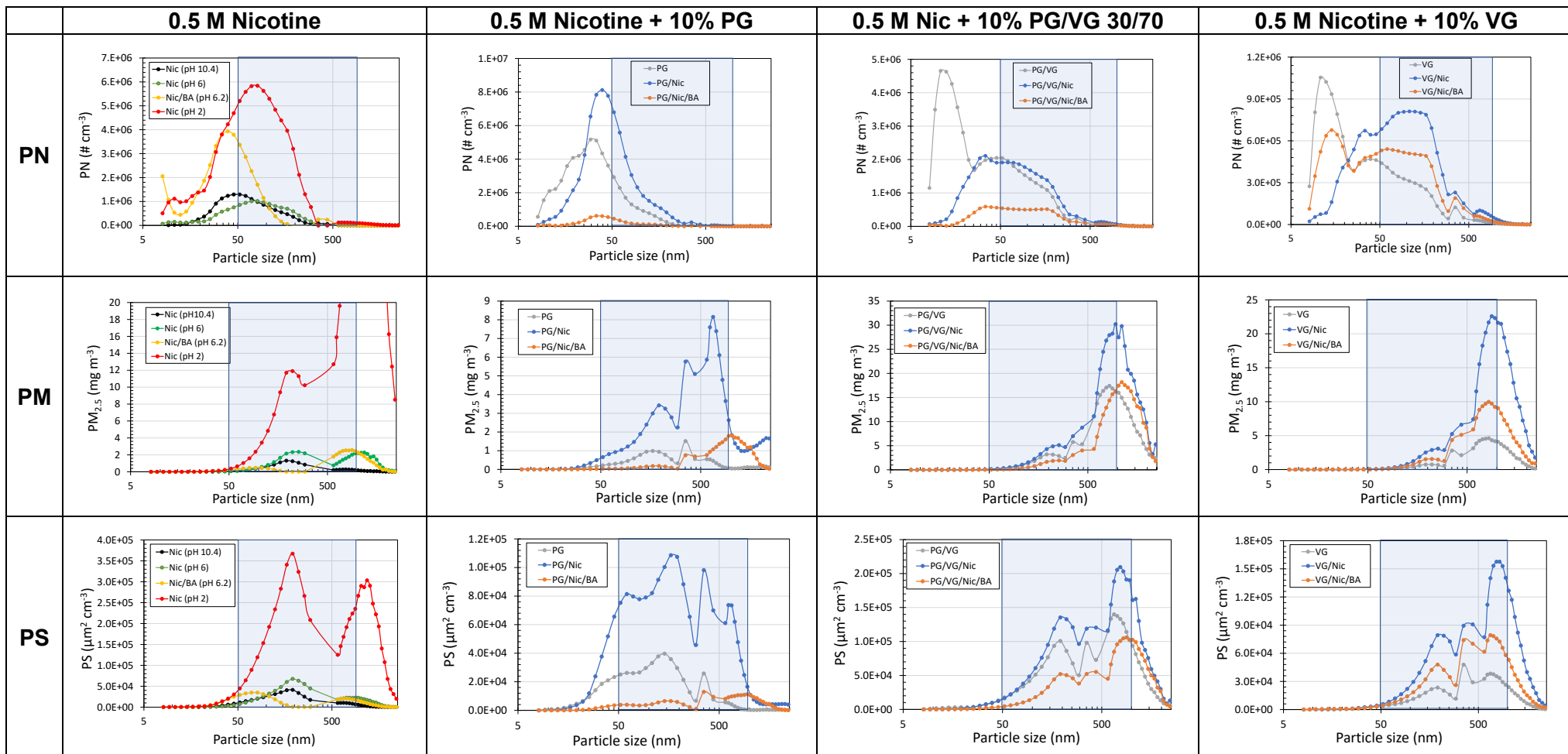
Figure 1: Size-resolved particle number (PN), mass (PM) and surface area (PS) concentrations determined for aerosols produced by nebulization of different aqueous solutions. The blue boxes indicate the X-ray analyzer inlet size range (50 nm – 1 μm).

X-ray spectroscopic analysis of nicotine protonation in aqueous aerosols. The extent of nicotine protonation in the aerosol particles was determined by XPS and NEXAFS, which allows for interrogation of the aerosol surface and the particle core, respectively. In XPS, we define the aerosol surface as the material encountered in the outermost layer of particles, at a depth of no more than 1 nm. This depth corresponds to the inelastic mean free path (IMFP) of primary electrons of 30 eV kinetic energy, generated via photoionization from core levels, typically used in this work. By contrast, NEXAFS spectra were collected from low energy secondary electrons generated via scattering of the primary electron with a longer IMFP, leading to a larger probing depth that reached the core of the aerosol particles.[26] To investigate the effect of protonation, solutions of aqueous nicotine 0.5 M at pH 10.4, 6, and 2, as well as a 0.5 M nicotine and 0.5 M BA aqueous solution (pH 6.2) were nebulized into the spectrometer for subsequent analysis. In all cases, the N1s level XPS was recorded with X-ray photons of 430 eV. The recorded spectra are presented in Figure 2A, and the parameters corresponding to the fitted curves are presented in Table S2 (Supporting Information). The N1s signal in all cases could be fitted by two partially-overlapping gaussian curves with maxima at 404.8 and 407.3 eV. To understand the nature of the N1s peaks, we turn to DFT calculations performed here and also to relevant literature on similar nitrogen containing molecules.

The bottom panel of Figure 2A corresponds to a Density-Functional Theory (DFT) calculation of the XPS spectrum for the free-base (Nic_{FB}) with a maximum at 403.1 eV, for a nicotine molecule protonated on the pyrrolidinic ring (Nic_P) with two maxima at 403.4 and 405.8 eV corresponding to an unprotonated pyridinic N atom and a protonated pyrrolydinic N atom, and for a 70%/30% combination of both. The DFT values are shifted by 1.8 eV on the absolute scale to overlap with the experimental results. The observed N1s shift of ~2 eV upon nicotine protonation is qualitatively similar to our previously reported observations for amino acids analyzed under similar conditions.[29, 30] Recently there have been a number of experimental[31, 32] and theoretical[33] studies exploring protonation of organic crystals containing the pyridinic moiety particularly on isonicotinamide. The results are very similar to what is observed here. For the neutral pyridinic system, albeit in the condensed organic crystal phase, there is a single peak, that splits into two upon protonation. Both experiment and theory show a binding energy shift upon protonation, to the blue of the neutral case. In our case, we postulate that the shift observed is on the pyrrolydinic nitrogen, however the above-mentioned analysis should be still valid since our experimental resolution and previous studies suggests that XPS is not sensitive enough to see the difference between these two nitrogen atoms. To confirm this, we performed additional calculations, to determine the binding energy of nicotine in the diprotonated form, and in this case, it is represented by a single peak at 406.0 eV, (see Table S2, and Figure S1) which is very close to that calculated for the protonated one (405.8 eV). While we cannot exclude the possibility that there could be some diprotonated nicotine within the second peak, our experimental results clearly demonstrate that the dominant form of nicotine is present

in the free base form. The fraction of neutral free-base nicotine, α_{FB}, was calculated in each case using Equation 1, by summing the corresponding areas of neutral and mono protonated fitted gaussian curves, and is reported in Table S3 (Supporting Information). Overall, presence of both free-base and protonated nicotine was observed in all tested conditions, with free-base nicotine predominating over the protonated species, with α_{FB} = 0.72 to 0.80 across this wide pH range. This is very different from what is observed in solution at low pH (high acidity), where the dominant form should be diprotonated nicotine.

The same aerosols were also analyzed by NEXAFS, to describe the nicotine speciation at the core of the particles. Results corresponding to the N K edge are presented in Figure 2B. While there are no X-Ray studies of nicotine in the aqueous phase and/or in the presence of alcohols, there are both experimental and theoretical studies on organic crystals that can help decipher the spectra and provide a qualitative analysis of the peak positions and shape. In the recent theoretical work of Ge et al.[33] who performed a quantum mechanical/molecular mechanical study on isonicotimide, calculated X-Ray absorption spectra was shown to be sensitive to proton transfer and the nature of hydrogen bonding. The theoretical work was also compared to the experimental and theoretical results obtained by Edwards et al.[34] Based on these two studies, we interpret the strong peak shown in Figure 2B for pH 10.4 at 399.0 eV emanating from the π_1* orbital of the pyridinyl nitrogen. In Figure 2B for pH 2, two peaks of almost equal intensity show up at 399.0 eV and 401.0 eV, the second peak originating from a π_2* orbital, with an absolute value of 399.1 eV. Ge et al.[33] suggest the second peak has major contribution from a protonated nitrogen orbital, with an absolute value of 401.2 eV calculated by theory. In addition, the peak shape at the post edge region between 400-415 eV shown in Figure 2B is captured very well by the theoretical calculations of Ge et al. for both NEXAFS spectra at low and high pH. This analysis provides compelling evidence that the core of the aerosol does show more protonation at a function of pH compared to what was obtained by XPS from the surface described earlier, as can be seen in the change in peak heights of the π_1* and π_2* peaks located at 399.0 and 401.0 eV respectively.

To separate the contributions from free-base and protonated nicotine and put our results on a more quantitative footing, we used literature spectra of pyridine and pyrrolidine molecules in the crystalline phase[35, 36] to generate a synthetic NEXAFS spectrum for nicotine in the absence of any literature values. Furthermore, since a protonated pyrrolidine spectrum was not available in the literature, we used instead the spectrum of the structurally similar sarcosine obtained in a liquid jet X-Ray absorption measurement.[37] These spectra were digitized, and a linear combination of these digitized spectra was used to construct nicotine and protonated nicotine surrogate spectra (see Figure S2, Supporting Information). From the calculated free-base and protonated nicotine signals, we obtained the fraction of neutral free-base, α_{FB}, reported in Table S3 (Supporting Information). Compared to the particle surface results, the fraction of free-base in the core of the particles was lower, and more sensitive to the solution pH, changing from α_{FB}

7

= 0.34 in basic medium to α_{FB} = 0.05 at the most acidic tested condition in agreement with the analysis of the π* peak analysis described earlier.
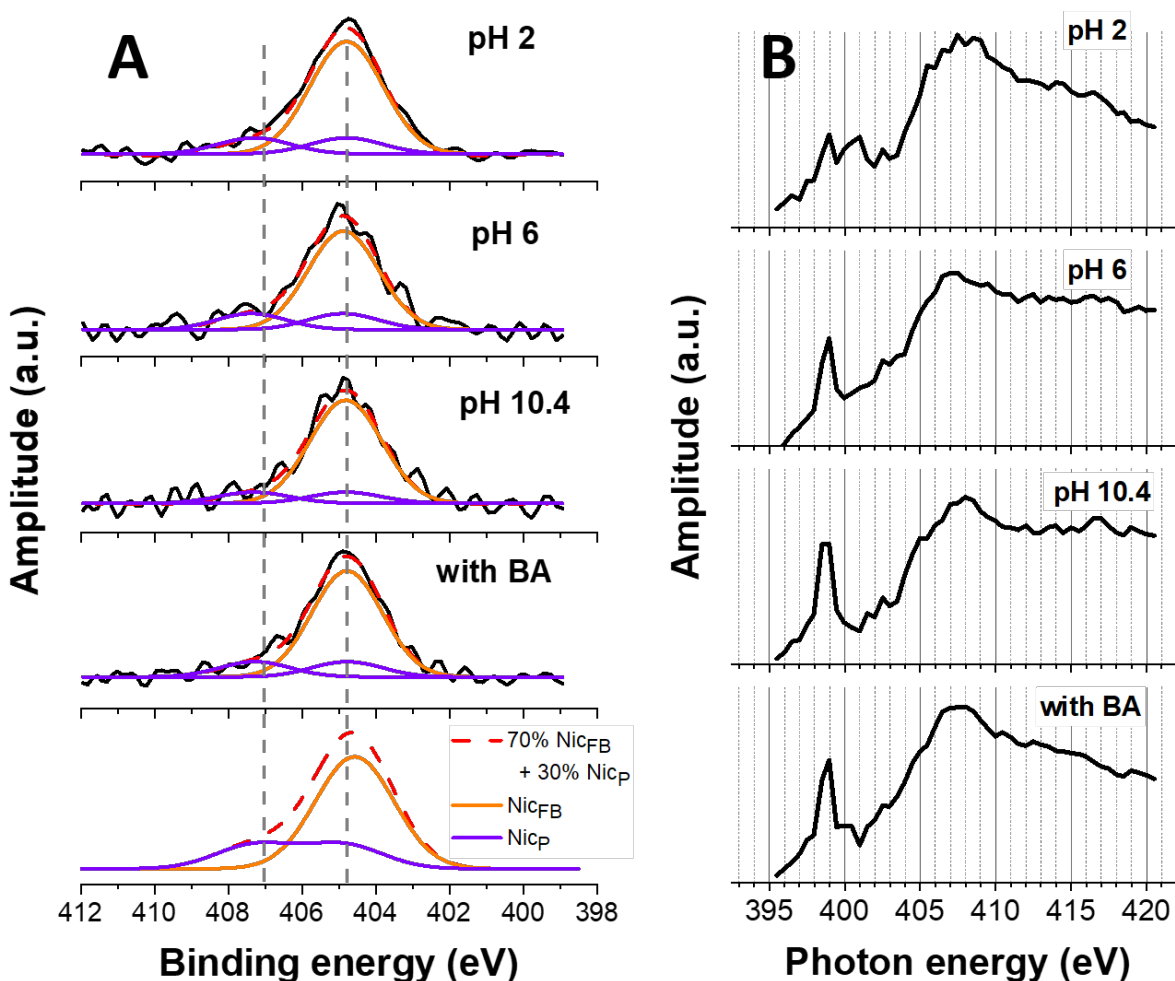

Figure 2: (A) N1s XPS spectra of aerosols generated by nebulizing aqueous solutions containing 0.5 M nicotine at pH 2, pH 6, pH 10.4, and a 0.5 M 1:1 mixture with benzoic acid (pH 6.2). The black line is the experimental spectra, and the dashed red line is a convolution of the free-base (orange) and protonated (purple) nicotine. The bottom panel corresponds to DFT-calculated spectra for free-base nicotine (Nic_{FB}), protonated nicotine (Nic_P) and a 70%/30% combination thereof. The DFT values are shifted by 1.8 eV on the absolute scale to overlap with the experimental results. (B) N K edge NEXAFS spectra of aerosols generated by nebulizing aqueous solutions containing 0.5 M nicotine at pH 2, pH 6, pH 10.4, and a 0.5 M 1:1 mixture with benzoic acid (pH 6.2).

Protonation of nicotine in PG and VG aqueous aerosols. C1s and N1s XPS spectra were also obtained for aerosols produced with aqueous mixtures containing a 10% (molar ratio) of PG, VG or a mixture thereof, and 0.5 M nicotine. The results are illustrated in Figure 3, and summarized in Table S4 (Supporting Information). In the N1s spectra (Figure 3A), the main observation was that the signal could be fit with a single gaussian curve, corresponding to free-base nicotine. Protonated nicotine was not observed on aerosol surfaces in the presence of 10% PG or VG. The same result was observed when BA was present, as shown in Figure S3 (Supporting Information) for the N1s XPS spectra. In the C1s XPS spectra (Figure 3B), shown only in the absence of BA, the gaussian curves could be adjusted corresponding to liquid and gas phase species. Liquid-phase species included free-base nicotine, which was fit to a curve centered at 289.8 eV, PG (290.5 eV) and VG (291.8 eV). For both PG and VG, a signal corresponding to gas phase species (grey curve) was detected at 294.5 eV, which is approximately 2 eV higher energy with respect to the liquid phase, consistent with our previous observations.[38]

The relative areas extracted from the C1S XPS spectra shown in figure 3B corresponding to these species were used to determine the ratio between nicotine and the sum of PG and VG in the particle surface, φ, as follows:

$$\varphi = \frac{[\text{Nic}]}{([\text{PG}]+[\text{VG}])} \qquad (2)$$

These values are reported in Table S5 (Supporting Information). In the particle surface, the relative concentration of nicotine with respect to PG ($\varphi = 0.10$), VG ($\varphi = 0.18$) or their 30/70 mixture ($\varphi = 0.10$) did not differ significantly from bulk aqueous solutions, $\varphi = 0.13$. In the presence of equimolar amounts of nicotine and BA, (data not shown), the shape of the C XPS spectra did not change dramatically, however given the complication of added BA, we did not attempt a fit. We surmise that BA does not affect nicotine concentration dramatically on the surface.
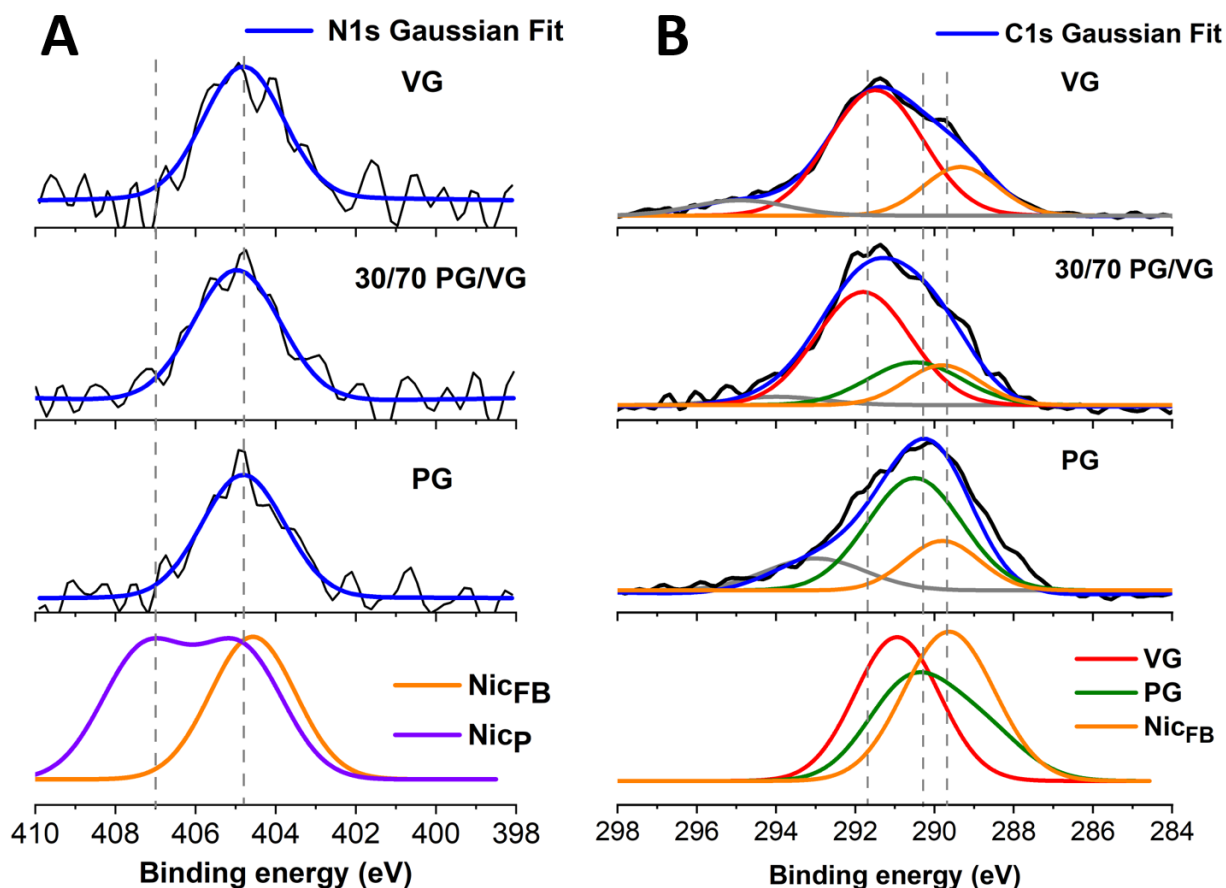
Figure 3: XPS spectra of aerosols generated by nebulizing 0.5 M nicotine aqueous solutions containing 10% PG, VG or their 30/70 mixture. (A) N1s XPS spectra of aerosols (black experimental data, blue Gaussian fit), and bottom panel in A is DFT-calculated spectra for free-base nicotine (Nic$_{FB}$, orange) and protonated nicotine (Nic$_P$, purple); (B) C1s XPS spectra of aerosols (black experimental data, blue is a Gaussian fit to glycerol (VG, red), propylene glycol (PG, green), free-base nicotine (Nic$_{FB}$, orange) and gas phase species (grey). The bottom panel in both correspond to DFT-calculated spectra, which are shifted by 1.8 eV on the absolute scale to overlap with the experimental results.
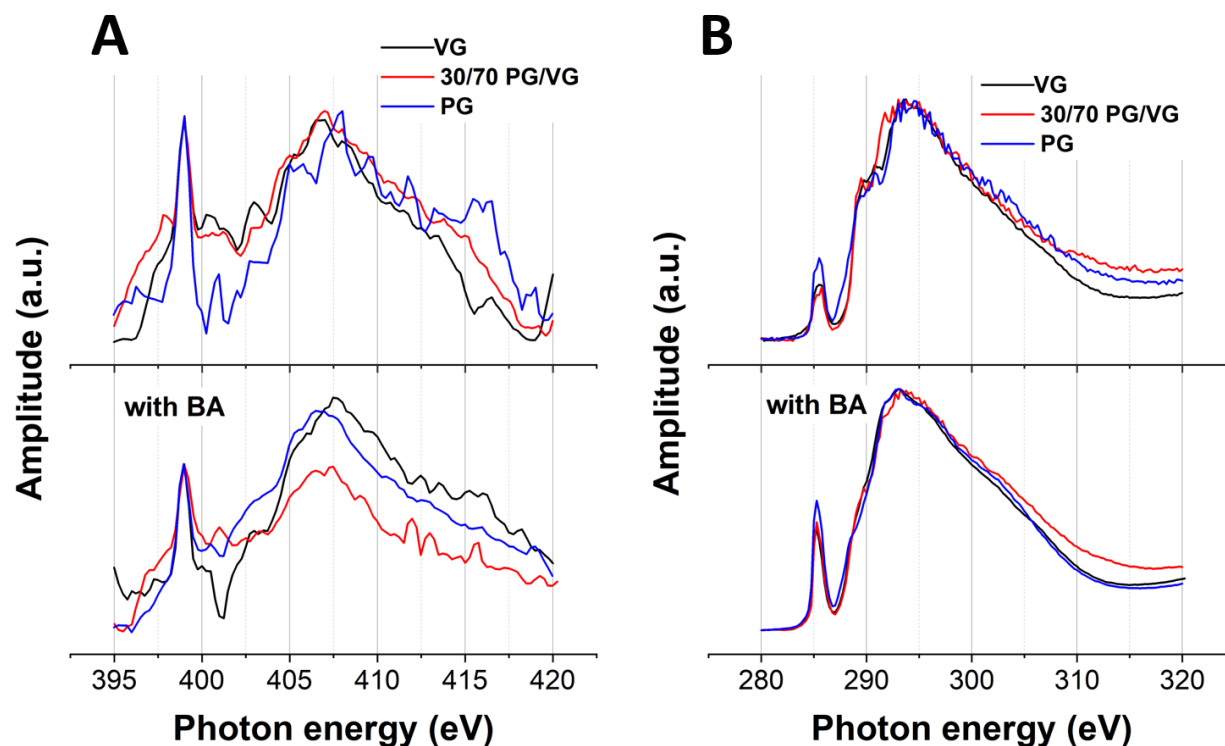
Figure 4: NEXAFS spectra of aerosols generated by nebulizing 0.5 M nicotine aqueous solutions containing 10% PG, 10% VG, or a 10% PG/VG (30/70) mixture. The bottom panels in (A) and (B) correspond to 0.5 M 1:1 nicotine/benzoic acid solutions. (A) N K edge; (B) C K edge

Figure 4 presents the NEXAFS spectra obtained for the N K and C K edges in aerosols generated from mixtures of 0.5 M nicotine aqueous solutions with 10% PG, 10% VG, or 10% of a PG/VG (30/70), all of which had a pH of 10.4. In addition, we also studied the addition of 0.5 M BA to each of those mixtures, with a pH of 6.2. The N K edge spectra were used to determine the fraction of neutral free-base, α_{FB}, corresponding to the core of aerosol particles, following the same procedure described above. The results are reported in Table S3 (Supporting Information).

Figure 5 summarizes the results obtained in this study, by plotting the free-base fraction α_{FB} as a function of the pH of the aerosolized solution. Aerosol conditions were compared with dilute aqueous solution by overlaying our results with the fraction of free-base, monoprotonated and diprotonated nicotine in bulk water, calculated from the acidity constants.
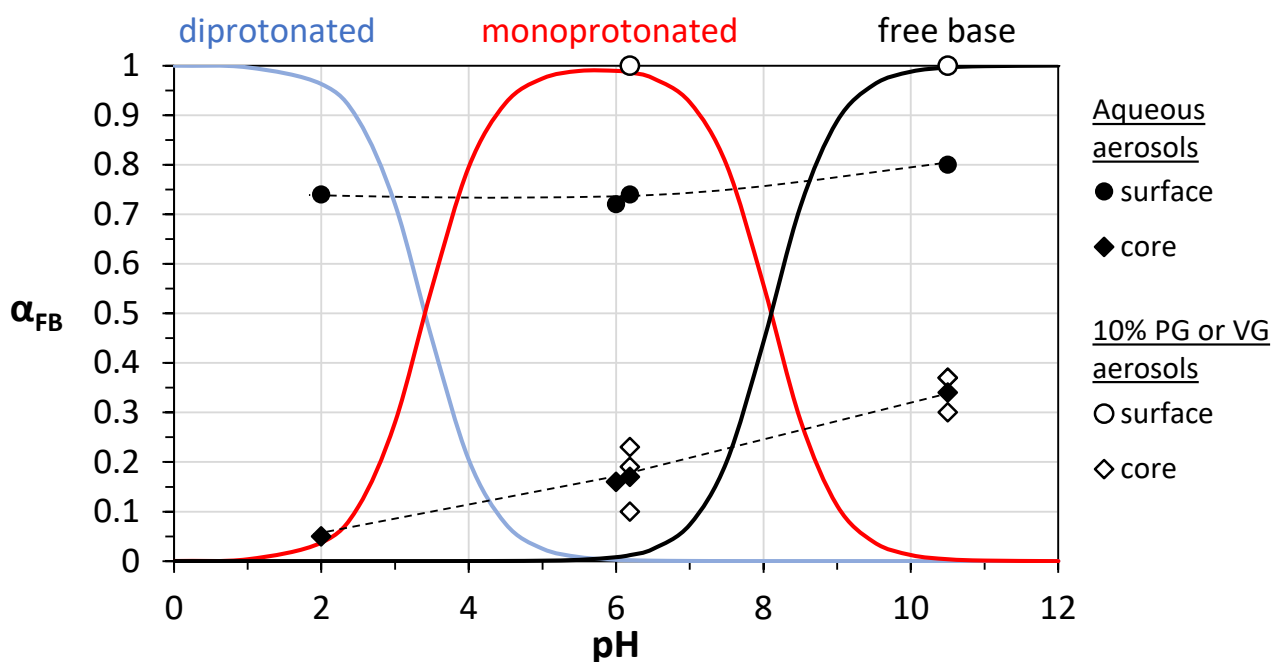
Figure 5: Fraction of nicotine free-base form α_{FB} in the surface and core of aerosol particles. Results are presented in the absence and presence of 10% PG, VG or PG/VG (30/70) mixture, as a function of the pH of the nebulized solution. Solid curves correspond to the fraction of free-base (black), monoprotonated (red) and diprotonated (blue) nicotine in bulk water. Experimental results shown in this figure are tabulated in Table S3 (Supporting Information).

The fraction of free-base nicotine determined in the particle core and surface show no correlation with the predicted behavior in diluted aqueous solution. We observed a higher α_{FB} in the aerosol surface than in the particle core, for all tested conditions. When aqueous solutions were aerosolized, the free-base fraction in the aerosol surface determined in the pH range from 2 to 10.4 was relatively constant, in the range $0.72 < \alpha_{FB} < 0.80$. However, when the solutions contained 10% PG and/or VG, nicotine was present in the aerosol surface exclusively as a neutral species (i.e., $\alpha_{FB} = 1$). In the absence of BA, this result was consistent with the predicted nicotine speciation in bulk aqueous solution at pH 10.4. However, when BA was added, the pH of the solution changed to 6.2, but the speciation on the aerosol surface remained unchanged. This effect could be attributed to a reduction in the hydration of ionic species at the surface induced by the presence of PG and VG, as discussed further below.

Considering the particle core analysis by NEXAFS, the nicotine free-base fraction was lower than those determined in the surface for all the tested mixtures. While α_{FB} was reduced with decreasing pH, the observed behavior was significantly different from the dilute aqueous solution, highlighting the fact that, even for relatively large particles (e.g., 1 µm diameter), these aerosols are far from conditions found in the bulk liquid. For experiments performed in the absence of PG and VG, at pH 10.4 we determined an α_{FB} = 0.34, which dropped to α_{FB} = 0.05 at pH 2. Hence, there is a much larger degree of protonation for the core of particles compared with bulk aqueous solutions in alkaline conditions (for which only the free-base is present in the bulk). By contrast, acidification resulted in an increasingly higher extent of protonation while retaining a non-negligible fraction of free-base nicotine, even at a very low pH.

In the presence of 10% PG, VG or PG/VG (30/70) mixture, the recorded α_{FB} in the particle core showed relatively minor deviations (in the order of a ±10% variance) with relation to the values measured for aerosols that did not contain PG or VG. The presence of these compounds did not have the same dramatic effect observed in particle surfaces. When BA was added to solutions containing 10% PG or VG changing the pH from alkaline to circum-neutral, the values of α_{FB} measured in the particle core were lower than those recorded in the absence of BA, following the same trends observed for solutions that did not contain PG or VG. We could not establish a significant difference in the effects caused by PG versus VG, as the variability of results in solutions with added BA was in the order of ±35%. The effect of added BA was comparable to that achieved by acidifying the solution to pH 6 by addition of HCl, suggesting that the effect due to the presence of BA is exclusively related to aqueous acid/base equilibrium rather than the formation of a specific adduct between nicotine and BA. For that reason, it is expected that other carboxylic acids used as additive in e-liquids such as levulinic, lactic, salicylic, malic, and tartaric acid[11] should have similar effects. For all these acidifiers, the main organoleptic properties imparted to e-cigarettes are related to delivering a high fraction of protonated nicotine, and maintaining protonation upon aerosol deposition and dissolution into saliva and the lining fluids of the respiratory system, both of which are strongly buffered at a neutral pH.[39, 40] In aerosols containing PG and/or VG, the fact that only free-base nicotine is present in the particle surface may accelerate its evaporation and deposition onto the respiratory tract, while possibly also increasing its harshness in the throat, even when acidifying agents are present. Next research efforts should involve *in vitro* and *in vivo* evaluation of the role played by PG, VG and acidic additives on nicotine deposition in the respiratory system, generating a quantitative understanding of their contribution to nicotine uptake. Our study provides insights onto relevant aerosol dosing and nicotine speciation, supporting such studies. The information gained on the effects of acidifiers used in e-liquid formulations can inform future regulatory measures (e.g., by the US Food and Drug Administration, FDA) aiming at minimizing the addictive properties of emerging vaping products.

This study contributes to a growing body of evidence illustrating differential acid-base properties at the surface of aerosol particles with respect to their core, and to bulk aqueous conditions. The protonation of nicotine in charged aqueous aerosol particles was not directly driven by solution-phase acidity. This is consistent with other observations. For example, interfacial reactions on aqueous microdroplets leading to protonation and uptake of gas phase molecules at the outermost layer have been used as probes to demonstrate that droplet surface conditions were close to Brønsted-neutral despite more acidic (i.e., pH 3 or 4) core conditions. This effect was attributed to reduced hydration of ionic species at the interface, forcing acids and bases toward their undissociated forms.[41-44] The presence of PG and VG in our experiments has likely amplified this effect, leading to the complete absence of protonated nicotine at the aerosol surface.[45]

To conclude, we have demonstrated that soft X-ray spectroscopy on vaping aerosols provide an exquisite picture on the degree of protonation of nicotine both at the surface and the core of the aerosol. The methods employed are applicable beyond vaping chemistry, such as probing acid-base behavior at the air-water interface which is of critical importance in atmospheric chemistry and ion transport and chemistry between interfaces relevant to materials chemistry.

Methods

Aerosol generation and characterization. A stable aerosol flow was produced by nebulizing different aqueous mixtures, using a TSI 3076 constant output atomizer with a 3 L min^{-1} flow of N_2 (20 psi). For each solution, the atomizer was operated for at least five minutes, producing a stable regime. All reported measurements were carried out during that steady-state period. Copper tubing was used to carry the aerosols from the atomizer to the nozzle. The solutions used to evaluate the effect of pH were prepared in water, by addition of nicotine (0.5 M) in all cases, and with addition of BA (0.5 M) or HCl (1 M) to adjust the pH to 6 or 2. Additional solutions were prepared in water mixed with a 10% (in moles) of PG, VG or a PG/VG 30/70 mixture, to which nicotine (0.5 M) or a 1:1 nicotine:BA mixture (0.5 M) was added. High purity PG (meeting USP testing specifications) and VG (>99.5%), nicotine (>99%) and BA (>99.5%) were from MilliporeSigma. The pH of solutions was measured with an Oakton Instruments pH 510 benchtop meter. The aqueous solutions were nebulized as-prepared. In X-ray spectroscopic studies, the aerosols were introduced into the test chamber through aerodynamic lenses, as described below.

For the size-resolved characterization of the generated aerosols, the atomizer was connected to a Teflon-made cylindrical mixing chamber (7.5 cm diameter, 12 cm high) with a ¼" copper tubing. The aerosol was diluted with filtered laboratory air (18 – 45 L min^{-1}) to avoid exceeding maximum particle concentration of the particle instruments. Diluted aerosol was sampled by three different aerosol instruments with a total flow rate of 12 L min^{-1} in a 3/8" copper tubing (residence time < 1s), when the

excess flow vented to a fume hood. Given the short transit time between the generator and the analyzers, there was no significant evaporation nor aggregation of particles. The size-resolved concentration of aerosols from different mixtures was characterized using a Fast Mobility Particle Sizer (FMPS) spectrometer (Model 3091, TSI Inc., MA), an Aerodynamic Particle Sizer spectrometer (APS, Model 3321, TSI Inc., MA), and an Optical Particle Sizer (OPS, Model 3330, TSI Inc., MA). The FMPS was operated at a flow rate of 10 L min^{-1} to minimize diffusion losses of ultrafine nanoparticles, and scanned the size distribution range between 5 and 500 nm at a rate of 1 Hz. The APS covered particle sizes between 500 nm and 20 µm and the OPS between 300 nm and 10 µm, in both cases at a sampling rate of 1 Hz. The FMPS electrometers were zeroed with ultra-zero air before each test, while the APS and OPS were checked with ultra-zero air to confirm that the measurement was zero. Digital outputs from all instruments were integrated into a single file covering the mass range 5 nm − 20 µm. The mass distribution of particles was calculated by assuming particle density as 1 g cm^{-3}, a reasonable assumption for aqueous aerosols.

Aerosol X-ray instrumentation. The different simulated e-liquids were nebulized in ambient conditions, generating an aerosol beam shaped by a 200 µm nozzle and an aerodynamic lens system, focused into an X-ray photoelectron spectrometer. The size range admitted to the spectrometer was 50 nm – 1 µm.[46] This size range is in good agreement with that of aerosol particles generated during vaping and inhaled by e-cigarette users.[28, 47-49] The particle beam was interrogated by X-rays from beamline 9.0.1 at the Advanced Light Source, Berkeley, and the resulting electrons were imaged with a velocity map imaging X-ray photoelectron spectrometer (VMI-XPS), providing both angular and energy information simultaneously. By measuring the kinetic energy, photoelectron spectroscopy of the surface of the aerosol could be achieved,[50] and by scanning the photon energy, X-ray absorption spectroscopy (NEXAFS) was performed, providing information on the bulk composition of the aerosol.[26] Background measurements were collected by filtering aerosols, to account for dark noise of the VMI. These background values were subtracted to signals measured during analyses of the different aerosols.

For XPS, the aerodynamic lens focuses the aerosols into the interaction region. The electron optics of the spectrometer allowed for detecting electrons with kinetic energy up to 50 eV. An MCP/Phosphor type detector was used, where the illuminations on the phosphor screen were detected by a CMOS camera, and were recorded as an image by a Labview program. Signal was averaged for 300 s of steady-state generation, and at least 3 images were acquired for each sample. For the C1s level XPS, 315 eV photon energy is used, and for the N1s level, 430 eV was used. O1s spectra were difficult to obtain due to dominance of water, and are not reported here. The background-subtracted image was reconstructed by a pBASEX algorithm to generate the photoelectron spectra, which were calibrated with gas-phase N_2 photoelectron spectra acquired at different photon energies. At a kinetic energy of ~ 30 eV, XPS can probe <1 nm depth of the aerosol particle.[26, 50]

The same setup was used for NEXAFS, by replacing the camera with a photo multiplier tube (PMT) focused to the center of the image, to only probe the secondary electron signal. The photon energy was scanned, while the PMT recorded the intensity of the signal. A photodiode was used to record the flux at each photon energy, used to normalize the PMT signal. Since NEXAFS is sensitive to the secondary electron signal, the core of the aerosol particle could be probed.

DFT calculation of spectral features.

Theoretical binding energies were calculated with the Q-Chem software (q-chem.com),[51] and molecules were constructed with IQmol interface (iqmol.org). The solvent in calculations was simulated explicitly by introducing several water molecules around the relevant molecules in the presence of the polarizable continuum model (PCM), which is used to model solvation effects. Previously we have used such a method to probe solvation in histidine and in ammonium nitrate aerosols.[30, 52] In this study, we used the ΔDFT approach to calculate electron binding energies. In this approach the calculations were performed in two steps: (1) by optimizing the geometry and finding energy of the initial molecule, and (2) by calculating energy of a molecule with a removed core (N1s or C1s) electron. The corresponding core electron binding energy was found as the difference between total energies of initial molecule and its final state with removed core electron. Both calculations were performed at the wB97XD/6-311g(d,p) level of theory. Counter ion was not added to the protonated forms. The optimized geometries are reported in Table S6 (Supporting Information). The spectra were constructed using the Origin mathematical software (https://www.originlab.com) and convoluted with a gaussian function. The convolution is used to broaden the calculated spectrum for better correlation with the experimental data.

The experimental and computational work was carried out following strict LBNL safety procedures. No unexpected or unusually high safety hazards were encountered.

Associated Content

Supporting Information: Particle number, mass and surface area concentrations, calculated photoelectron spectra for N1s XPS of nicotine, α_{FB} determined for different experimental conditions, additional information from XPS and NEXAFS spectra, mole concentration ratio between nicotine and PG+VG, and optimized structures used in DFT calculations.

Acknowledgements

References

(1)   Cancelada, L.; Sleiman, M.; Tang, X. C.; Russell, M. L.; Montesinos, V. N.; Litter, M. I.; Gundel, L. A.; Destaillats, H., Heated Tobacco Products: Volatile Emissions and Their Predicted Impact on Indoor Air Quality. *Environ. Sci. Technol.* **2019,** *53*, 7866-7876.

(2)   Logue, J. M.; Sleiman, M.; Montesinos, V. N.; Russell, M. L.; Litter, M. I.; Benowitz, N. L.; Gundel, L. A.; Destaillats, H., Emissions from Electronic Cigarettes: Assessing Vapers' Intake of Toxic Compounds, Secondhand Exposures, and the Associated Health Impacts. *Environ. Sc.i Technol.* **2017,** *51*, 9271-9279.

(3)   Sleiman, M.; Logue, J. M.; Montesinos, V. N.; Russell, M. L.; Litter, M. I.; Gundel, L. A.; Destaillats, H., Emissions from Electronic Cigarettes: Key Parameters Affecting the Release of Harmful Chemicals. *Environ. Sci. Technol.* **2016,** *50*, 9644-9651.

(4)   Strongin, R. M., E-Cigarette Chemistry and Analytical Detection. *Annu. Rev. Anal. Chem.* **2019,** *12*, 23-39.

(5)   Duell, A. K.; Pankow, J. F.; Peyton, D. H., Nicotine in tobacco product aerosols: 'It's déjà vu all over again'. *Tobacco Control* **2020,** *29*, 656-662.

(6)   Talih, S.; Salman, R.; El-Hage, R.; Karam, E.; Karaoghlanian, N.; El-Hellani, A.; Saliba, N. A.; Shihadeh, A., Characteristics and toxicant emissions of JUUL electronic cigarettes. *Tobacco Control* **2019,** *28*, 678-680.

(7)   Talih, S.; Salman, R.; El-Hage, R.; Karam, E.; Salam, S.; Karaoghlanian, N.; El-Hellani, A.; Saliba, N. A.; Shihadeh, A., A comparison of the electrical characteristics, liquid composition, and toxicant emissions of JUUL USA and JUUL UK e-cigarettes. *Scientific Reports* **2020,** *10*, 7322.

(8)   Bonner, E.; Chang, Y.; Christie, E.; Colvin, V.; Cunningham, B.; Elson, D.; Ghetu, C.; Huizenga, J.; Hutton, S. J.; Kolluri, S. K.; Maggio, S.; Moran, I.; Parker, B.; Rericha, Y.; Rivera, B.

N.; Samon, S.; Schwichtenberg, T.; Shankar, P.; Simonich, M. T.; Wilson, L. B.; Tanguay, R. L., The chemistry and toxicology of vaping. *Pharmacology & Therapeutics* **2021,** *225,* 107837.

(9)   Page, M. K.; Goniewicz, M. L., New analytical method for quantifying flavoring chemicals of potential respiratory health risk concerns in e-cigarette liquids. *Frontiers in Chemistry* **2021,** *9*, 763940.

(10)   Pankow, J. F.; Kim, K.; McWhirter, K. J.; Luo, W.; Escobedo, J. O.; Strongin, R. M.; Duell, A. K.; Peyton, D. H., Benzene formation in electronic cigarettes. *PLoS ONE* **2017,** *12(3)*, e0173055.

(11)   Harvanko, A. M.; Havel, C. M.; Jacob III, P.; Benowitz, N. L., Characterization of nicotine salts in 23 electronic cigarette refill liquids. *Nicotine Tob. Res.* **2020,** *22*, 1239-1243.

(12)   Bourgart, E.; Leclerc, L.; Pourchez, J.; Sleiman, M., Toward better characterization of a free-base nicotine fraction in e-liquids and aerosols. *Chem. Res. Toxicol.* **2022,** *35(7)*, 1234-1243.

(13)   Duell, A. K.; Pankow, J. F.; Peyton, D. H., Free-Base Nicotine Determination in Electronic Cigarette Liquids by H-1 NMR Spectroscopy. *Chem. Res. Toxicol.* **2018,** *31*, 431-434.

(14)   Omaiye, E. E.; McWhirter, K. J.; Luo, W. T.; Pankow, J. F.; Talbot, P., High-Nicotine Electronic Cigarette Products: Toxicity of JUUL Fluids and Aerosols Correlates Strongly with Nicotine and Some Flavor Chemical Concentrations. *Chem. Res. Toxicol.* **2019,** *32*, 1058-1069.

(15)   Benowitz, N. L., The central role of pH in the clinical pharmacology of nicotine: Implications for abuse liability, cigarette harm reduction and FDA regulation. *Clin. Pharmacol. Ther.* **2022,** *111(5)*, 1004-1006.

(16)   Goniewicz, M. L.; Boykan, R.; Messina, C. R.; Eliscu, A.; Tolentino, J., High exposure to nicotine among adolescents who use Juul and other vape pod systems ('pods'). *Tobacco Control* **2019,** *28*, 676-677.

(17)   Rosbrook, K.; Green, B. G., Sensory effects on menthol and nicotine in an e-cigarette. *Nicotine Tob. Res.* **2016,** *18*, 1588-1595.

(18)   Voos, N.; Goniewicz, M. L.; Eissenberg, T., What is the nicotine delivery profile of electronic cigarettes? *Expert Opinion on Drug Delivery* **2019,** *16*, 1193-1203.

(19)   Pankow, J. F.; Tavakoli, A. D.; Luo, W.; Isabelle, L. M., Percent free base nicotine in the tobacco smoke particulate matter of selected commercial and reference cigarettes. *Chem. Res. Toxicol.* **2003,** *16*, 1014-1018.

(20)   Pankow, J. F., A consideration of the role of gas/particle partitioning in the deposition of nicotine and other tobacco smoke compounds in the respiratory tract. *Chem. Res. Toxicol.* **2001,** *14*, 1465-1481.

(21)   Pankow, J. F.; Duell, A. K.; Peyton, D. H., Free-base nicotine fraction alphaFB in non-aqueous versus aqueous solutions: Electronic cigarette fluids without versus with dilution with water. *Chem. Res. Toxicol.* **2020,** *33*, 1729-1735.

(22)   El-Hellani, A.; El-Hage, R.; Baalbaki, R.; Salman, R.; Talih, S.; Shihadeh, A.; Saliba, N. A., Free-base and protonated nicotine in electronic cigarette liquids and aerosols. *Chem. Res. Toxicol.* **2015,** *28*, 1532-1537.

(23)   Stepanov, I.; Fujioka, N., Bringing attention to e-cigarette pH as an important element for research and regulation. *Tobacco Control* **2015,** *24*, 413-414.

(24)   Lisko, J. G.; Tran, H.; Stanfill, S. B.; Blount, B. C.; Watson, C. H., Chemical composition and evaluation of nicotine, tobacco alkaloids, pH and selected flavors in e-cigarette cartridges and refill solutions. *Nicotine Tob. Res.* **2015,** *17(10)*, 1270-1278.

(25)   Sosnowski, T. R.; Odziomek, M., Particle size dynamics: Toward a better understanding of electronic cigarette aerosol interactions with the respiratory system. *Front. Physiol.* **2018,** *9*, 853.

(26)   Kostko, O.; Xu, B.; Jacobs, M. I.; Ahmed, M., Soft X-ray spectroscopy of nanoparticles by velocity map imaging. *J. Chem. Phys.* **2017,** *147*, 013931.

(27)   Broniarz-Press, L.; Sosnowski, T. R.; Matuszak, M.; Ochowiak, M.; Jablczynska, K., The effect of shear and extensional viscosities on atomization of Newtonian and non-Newtonian fluids in ultrasonic inhaler. *Int. J. Pharmaceutics* **2015,** *485*, 41-49.

(28)   Li, L.; Lee, E. S.; Nguyen, C.; Zhu, Y., Effects of propylene glycol, vegetable glycerin, and nicotine on emissions and dynamics of electronic cigarette aerosols. *Aerosol Science and Technology* **2020,** *54(11)*, 1270-1281.

(29)   Xu, B.; Jacobs, M. I.; Kostko, O.; Ahmed, M., Guanidinium Group Remains Protonated in a Strongly Basic Arginine Solution. *Chemphyschem* **2017,** *18*, 1503-1506.

(30)   Kostko, O.; Xu, B.; Ahmed, M., Local electronic structure of histidine in aqueous solution. *Phys. Chem. Chem. Phys.* **2021,** *23*, 8847-8853.

(31)   Edwards, P. T.; Saunders, L. K.; Pallipurath, A. R.; Britton, A. J.; Willneff, E. A.; Shotton, E. J.; Schroeder, S. L. M., Proton transfer on the edge of the salt/cocrystal continuum: X-Ray photoelectron spectroscopy of three isonicotinamide salts. *Cryst. Growth Des.* **2021,** *21(11)*, 6332-6340.

(32)   Stevens, J. S.; Byard, S. J.; Seaton, C. C.; Sadiq, G.; Davey, R. J.; Schroeder, S. L. M., Proton transfer and hydrogen bonding in the organic solid state: A combined XRD/XPS/ssNMR study of 17 organic acid-base complexes. *Phys. Chem. Chem. Phys.* **2014,** *16*, 1150-1160.

(33)   Ge, G.; Zhang, J.-R.; Wang, S.-Y.; Wei, M.; Hua, W., A QM/MM study on the X-Ray spectra of organic proton transfer crystals of isonicotinamides. *J. Phys. Chem. C* **2022,** *126(37)*, 15849-15863.

(34)   Edwards, P. T.; Saunders, L. K.; Grinter, D. C.; Ferrer, P.; Held, G.; Shotton, E. J.; Schroeder, S. L. M., Determination of H-atom positions in organic crystal structures by NEXAFS combined with density functional theory: A study of two-component systems containing isonicotinamide. *J. Phys. Chem. A* **2022,** *126(19)*, 2889-2898.

(35)   Newbury, D.; Ishii, I.; Hitchcock, A. P., Inner shell electron-energy loss spectroscopy of some heterocyclic molecules. *Can. J. Chem.* **1986,** *64(6)*, 1145-1155.

(36)   Stevens, J. S.; Newton, L. K.; Jaye, C.; Muryn, C. A.; Fischer, D. A.; Schroeder, S. L. M., Proton transfer, hydrogen bonding, and disorder: Nitrogen near-edge X-ray absorption fine structure and X-ray photoelectron spectroscopy of bipyridine-acid salt and co-crystals. *Cryst. Growth Des.* **2015,** *15(4)*, 1776-1783.

(37)   Uejio, J. S.; Schwartz, C. P.; Duffin, A. M.; England, A.; Prendergast, D.; Saykally, R. J., Monopeptide versus monopeptoid: Insights on structure and hydration of aqueous alanine and sarcosine via X-ray absorption spectroscopy. *J. Phys. Chem. B* **2010,** *114(13)*, 4702-4709.

(38)   Weeraratna, C.; Amarasinghe, C.; Luo, W.; Ahmed, M., A direct probe of the hydrogen bond network in aqueous glycerol aerosols. *J. Phys. Chem. Lett.* **2021,** *12, 23*, 5503-5511.

(39)   Bardow, A.; Moe, D.; Nyvad, B.; Nauntofte, B., The buffer capacity and buffer systems of human whole saliva measured without loss of CO2. *Archives of Oral Biology* **2000,** *45(1)*, 1-12.

(40)   Ng, A. W.; Bidani, A.; Heming, T. A., Innate host defense of the lung: Effects of lung-lining fluid pH. *Lung* **2004,** *182*, 293-317.

(41)   Colussi, A. J.; Enami, S.; Ishizuka, S., Hydronium ion acidity above and below the interface of aqueous microdroplets. *ACS Earth Space Chem.* **2021,** *5(9)*, 2341-2346.

(42)   Enami, S.; Hoffmann, M. R.; Colussi, A. J., Proton availability at the air/water interface. *J. Phys. Chem. Lett.* **2010,** *1*, 1599-1604.

(43)   Eugene, A. J.; Pillar-Little, E. A.; Colussi, A. J.; Guzman, M. I., Enhanced acidity of acetic and pyruvic acids on the surface of water. *Langmuir* **2018,** *34*, 9307-9313.

(44)   Mishra, H.; Enami, S.; Nielsen, R. J.; Stewart, L. A.; Hoffmann, M. R.; Goddart III, W. A.; Colussi, A. J., Brønsted basicity of the air–water interface. *Proc. Nat. Acad. Sci. USA* **2012,** *109(46)*, 18679-18683.

(45)   Ojakivi, M.; Liigand, J.; Kruve, A., Modifying the acidity of charged droplets. *Chemistry Select* **2018,** *3*, 335-338.

(46)   Shu, J.; Wilson, K. R.; Ahmed, M.; Leone, S. R., Coupling a versatile aerosol apparatus to a synchrotron: Vacuum ultraviolet light scattering, photoelectron imaging, and fragment free mass spectrometry. *Rev. Sci. Instrum.* **2006,** *77(4)*, 3106-043106.

(47)   Floyd, E. L.; Queimado, L.; Wang, J.; Regens, J. L.; Johnson, D. L., Electronic cigarette power affects count concentration and particle size distribution of vaping aerosol. *PLoS ONE* **2018,** *13(12)*, e0210147.

(48)   Son, Y.; Mainelis, G.; Delnevo, C.; Wackowski, O.; Schwander, S.; Meng, Q., Investigating e-cigarette particle emissions and human airway depositions under various e-cigarette-use conditions. *Chem. Res. Toxicol.* **2020,** *33*, 343-352.

(49)   Zervas, E.; Litsiou, E.; Konstantopoulos, K.; Poulopoulos, S.; Katsaounou, P., Physical characterization of the aerosol of an electronic cigarette: impact of refill liquids. *Inhalation Toxicology* **2018,** *30(6)*, 218-223.

(50)   Kostko, O.; Jacobs, M. I.; Xu, B.; Wilson, K. R.; Ahmed, M., Velocity map imaging of inelastic and elastic low energy electron scattering in organic nanoparticles. *J. Chem. Phys.* **2019,** *151*, 184702.

(51)   Shao, Y.; Gan, Z.; Epifanovsky, E.; al, e., Advances in molecular quantum chemistry contained in the Q-Chem 4 program package. *Mol. Phys.* **2015,** *113(2)*, 184-215.

(52)   Weeraratna, C.; Kostko, O.; Ahmed, M., An investigation of aqueous ammonium nitrate aerosols with soft X-ray spectroscopy. *Mol. Phys.* **2022,** *120(1-2)*, e1983058.